A three-dimensional approach to pennation angle estimation for human skeletal muscle

Dongwoon Lee[a], Zhi Li[b], Zain Sohail[b], Ken Jackson[a], Eugene Fiume[a], Anne Agur[b]

[a]*Department of Computer Science, University of Toronto, Toronto, Ontario, Canada*
[b]*Department of Surgery, University of Toronto, Toronto, Ontario, Canada*

Abstract

Pennation angle (PA), defined as the angle between a fascicle's orientation and the tendon axis, is an important muscle characteristic that plays a significant role in determining a fascicle's force contribution to skeletal movement. As fascicles form complex and variable structures within a muscle, it is evident that PA varies regionally (e.g., proximal to distal, or superficial to deep) and that its non-uniformity has an effect on functional properties. Due to the limited visibility and image resolution, radiological assessments, such as magnetic resonance imaging (MRI) and ultrasonography, yield only an average measurement of PA for an entire muscle. As a result, PA is often assumed to be uniform within a muscle and its variation is rarely accounted for in most clinical and biomechanical studies. Thus, the purpose of our study is to investigate region-specific variation of PA throughout a muscle and develop a reliable quantification method for this variation. To this end, three-dimensional architectural data were acquired from cadaveric specimens. They were reconstructed throughout the volume of muscle and analyzed to assess spatial distribution of PA. More specifically, the geometric arrangement of the fascicle attachments, such as position and derivatives, was carefully examined to approximate the tendon axis (i.e., the line-of-action) and fascicle orientation, which were used to estimate PA for each fascicle. Our study shows that PA does indeed vary regionally throughout a muscle and that this variation may be characterized in relation to anatomical axes.

Keywords: skeletal muscle; muscle architecture; pennation angle; line of action; digitization.

1. Introduction

The physiological and mechanical functions of muscle are characterized by associated architectural parameters, such as thickness, fascicle length, pennation angle and physiological cross-sectional area [23]. Specifically, pennation angle (PA) is an important determinant of the contribution that muscle fascicles make to the force acting along the line of action. PA is defined as the angle between the orientation of a fascicle and the attached tendon axis (i.e., the line of action) (see Figure 1(a)).

For each fascicle i, its PA is simply calculated as

$$\mathrm{PA}^i = \cos^{-1}(\text{line of action} \cdot \text{fascicle orientation}^i). \quad (1)$$

As the muscle fascicle force, $\mathbf{f}_m^i$, is in the direction of the fascicle orientation and the tendon force, $\mathbf{f}_t$, is in the direction of the line of action, their functional relation is expressed as

$$\mathbf{f}_t = \sum_i \mathbf{f}_m^i \cos(\mathrm{PA}^i). \quad (2)$$

Since fascicles have variable length and arrangement within a muscle, the associated PA differs from fascicle to fascicle [4, 20, 10]. Due to the limited visibility and image resolution, radiological assessments, such as magnetic resonance imaging (MRI) and ultrasonography, yield only an average measurement of PA for an entire muscle. In practice, PA is measured as the acute angle between two intersecting lines representing fascicle orientation and a deep aponeurosis (see Figure 1(b)). Anisotropic features in the longitudinal images are manually identified to approximate those lines. Ultrasonography is widely used in many clinical and biomechanical studies, because it is portable and applicable to dynamic measurements, such as muscle contraction. However, the accuracy of the calculation relies on the alignment of the imaging plane [2, 15].

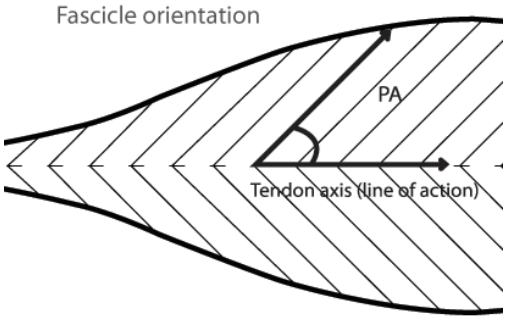

(a)

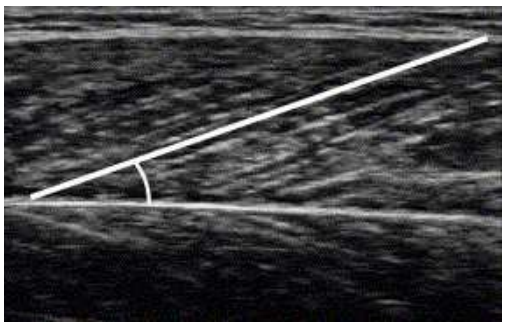

(b)

Figure 1: Pennation angle. (a) Schematic of definition. (b) Measurement on an ultrasonographic image.

Furthermore, a two-dimensional measurement may be inaccurate, because identifiable features are obtained from the intersection of the imaging plane and the three-dimensional architecture.

Apart from the estimation of PA, some computational approaches based on MRI have been employed to determine the line of action of a muscle [19, 7]. The line of action is represented as the longitudinal axis of a muscle that is approximated by the center line connecting the geometric centers of all sectional slices. However, this method requires prior knowledge of the sectioning plane. Koolstra et al. [7] improved on this approach by using a regression technique that is more consistent over choices of the sectional plane. Since the underlying architecture is not accounted for, the method may yield poor estimates of the line of action for pennate muscles, because the distal tendon axis is commonly chosen to represent the line of action.

In contrast to radiological assessments, using cadaveric specimens allow the investigation of locally detailed variation of PA. Lieber et al. [10], Murray et al. [13] and Ward et al. [22] collected a small number of fascicles from specimen surfaces and measured PA using a hand-held goniometer or protractor. Although their direct measurements would in principle be more accurate than radiological assessments, any region or volume specific variation was not quantified. On the other hand, Agur et al. [1], Kim et al. [6], Rosatelli et al. [17], Ravichandiran et al. [16] and Lee et al. [8] used a volumetric method to estimate PA. Fascicles were densely and volumetrically collected through dissection and digitization procedures, and then geometrically reconstructed. In those studies, the longitudinal axis of the muscle was accounted for and the line of action was determined as an average orientation of all fascicles. PA was then calculated as the relative angle between this axis and the fascicle orientation. This approximation may still fail if it is inconsistent with the underlying muscle architecture. For example, in pennate muscles, this muscle axis may not coincide with the tendon axis, because fascicles run parallel to one another, but they are variably oblique to the attached tendon axis (see Figure 2). Therefore, for consistent quantification, PA must be estimated with respect to the tendon axis. Digitizing tendons may be an immediate solution for this problem, but certain types of tendons, such as intramuscular tendons and separate aponeurosis, may have irregular shapes and arrangements that would impose some difficulties in their reconstruction.

Figure 2: Problematic line of action estimation. Average orientation of fascicles is apparently oblique to the patellar tendon, the axis of which is directed horizontally in the given configuration.

The purpose of our study is to investigate detailed and region-specific variation of PA throughout a muscle and to develop a reliable quantification method. Three-dimensional architectural data are acquired from cadaveric specimens, reconstructed in dense and volumetric form and analyzed to assess spatial distribution of PA. More specifically, we carefully examine the geometric arrangement of fascicle attachments, such as their spatial distribution of position and direction. From our specimen data, we observe that fascicle attachments re-

veal directionality of attached tendons. In pennate muscles, these attachments are strongly arranged in linear form. This is not the case for non-pennate muscles, as explained in Section 2.3. Therefore, the geometric arrangement of these attachments is used to approximate the line of action and fascicle orientation, and thereafter to estimate PA for each fascicle. Our work shows region-specific variation of PA throughout the muscle. Furthermore, we demonstrate that this variation may be characterized with respect to anatomical axes.

2. Methods

Our study is based on cadaveric specimen data obtained through serial dissection and digitization procedures. Fascicles were collected and geometrically reconstructed to represent the muscle architecture. Based on the reconstructed architecture, the geometric arrangement of fascicle attachments was used to estimate PA.

2.1. Data acquisition for muscle specimens

Our experimental data are acquired from a variety of muscles including two lower extremity muscles: abductor hallucis (ABH) and vastus medialis (VM) and sixteen upper extremity muscles: anconeus (ANC), abductor pollicis longus (APL), brachialis (BR), extensor carpi radialis bevis (ECRB), extensor carpi radialis longus (ECRL), extensor carpi ulnaris (ECU), extensor digitorum (ED), extensor digitorum (EDM), extensor indicis (EI), extensor pollicis brevis (EPB), extensor pollicis longus (EPL), flexor carpi ulnaris (FCU), pectoralis major (PM), pronator teres (PT), pronator quadratus (PQ), supraspinatus (SS). Muscle specimens with visible abnormalities, such as muscle atrophy, fat infiltration or surgery, were excluded from the data acquisition. During dissection and digitization, associated joints were stabilized into anatomical position with metal plates and screws. Fascicles were sequentially dissected and digitized from superficial to deep throughout the muscle volume. A MicroScribe G2 digitizer with 0.23 mm accuracy was used to mark trajectories of fascicles with sampled points. Digitized fascicles were removed, exposing the underlying fascicles about $1-2$ mm deeper. To identify fascicles accurately, a surgical microscope was used throughout dissection and digitization process. [1]

[1] Ethics approval was obtained from the Research Ethics Board at the University of Toronto (Protocol Reference Number: 27210).

2.2. Orientation of fascicles

Using the digitized points, each fascicle is first approximated by a smooth piecewise cubic spline, $\mathbf{p}(u) = (x(u), y(u), z(u))$, where $u \in [0, 1]$. The orientation of a fascicle is represented by a series of tangent vectors, $\mathbf{p}'(u) = (x'(u), y'(u), z'(u))$, along the curves (See Figure 3).

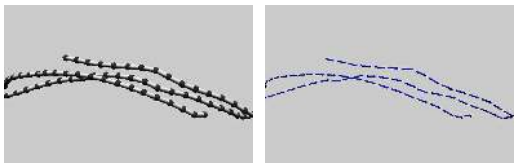

(a) (b)

Figure 3: Representation of fascicles. (a) Spline curves and resampled points, $\mathbf{p}$. (b) Tangents, $\mathbf{p}'$, evaluated along the curves.

Using an arc-length parameterization, fascicle points are redistributed (i.e., resampled) to make the curve representation uniform [8]. As reconstructed spline curves are clamped at their ends (i.e., tendinous attachments), tangent vectors at these points must be approximated from neighboring points, using formulas such as $\mathbf{p}'(0) \approx (\mathbf{p}(u_1) - \mathbf{p}(u_0))/(u_1 - u_0)$ and $\mathbf{p}'(1) \approx (\mathbf{p}(u_n) - \mathbf{p}(u_{n-1}))/(u_n - u_{n-1})$. To determine proximal and distal orientation, previous studies [16, 8] simply chose tangent vectors evaluated at the end points (i.e., approximations to $\mathbf{p}'(0)$ and $\mathbf{p}'(1)$). However, positions of tendinous attachments may be slightly perturbed due to errors that may occur in the dissection and digitization procedure. This may affect the angular measurement in (1). For more reliable quantification, we take an average of the tangent fields evaluated over a local area close to these attachments. More specifically, for each fascicle i, the averaged tangent vectors for proximal, $\overline{\mathbf{t}_p^i}$, and distal, $\overline{\mathbf{t}_d^i}$, orientations are calculated as

$$\overline{\mathbf{t}_p^i} = \frac{1}{n_p} \sum_{u=0}^{u_p} \mathbf{t}^i(u) \tag{3}$$

$$\overline{\mathbf{t}_d^i} = \frac{1}{n_d} \sum_{u=u_d}^{1} \mathbf{t}^i(u) \tag{4}$$

where $\mathbf{t}^i(u)$ is the tangent vector for fascicle i defined at the point $\mathbf{p}(u)$, n_p and n_d are the number of points in the local proximal and distal regions, respectively, and $u \in [0, ..., u_p, ..., u_d, ..., 1]$. In practice, we choose $0.15 - 0.2$ for u_p and $0.8 - 0.85$ for u_d, whence approximately $15-20\%$ of the entire fascicle length is included in each of the proximal and distal regions.

2.3. Line of action

The line of action of a muscle can be approximated by the long axis of the internal tendon onto which the fascicles attach. For non-pennate muscles, such as fusiform and parallel muscles, the average direction of collective forces exerted by all fascicles is parallel, or nearly parallel, to the axis of the attached tendon. Thus, the line of action can be approximated as [16, 8]

$$\begin{aligned} \text{line of action}_p &= \frac{1}{n}\sum_{i=1}^{n}\overline{\mathbf{t}_p^i} \\ \text{line of action}_d &= \frac{1}{n}\sum_{i=1}^{n}\overline{\mathbf{t}_d^i} \end{aligned} \tag{5}$$

where n is the number of fascicles. This approach, based on Equation (5), is conceptually similar to the method described in [7]: the estimated center line corresponds to an average direction of all fascicles (see Figure 4). However, equation (5) may be inappropriate for pennate muscles, because fascicles are often oblique, rather than parallel, to attached tendons. Thus, the averaged direction of fascicles may produce a poor estimate of the line of action (see Figure 2). Digitized tendons or aponeuroses could be used to determine the line of action, but, compared to fascicle data, they are often observed to be irregular and non-homogeneous in terms of arrangement or shape. Thus, the fascicle data may be more straightforward and simpler to deal with computationally.

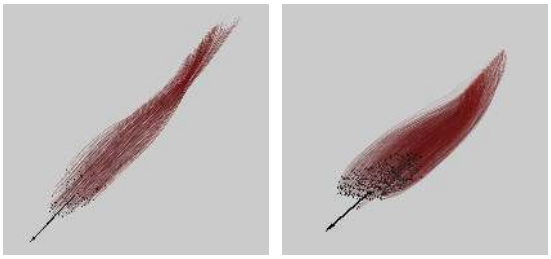

(a) (b)

Figure 4: Estimated line of action (black arrow) and distal attachments (black dots) of fascicles (red) for fusiform muscle. (a) Brachioradialis. (b) Extensor carpi radialis longus.

From our specimen data, we observe that the geometric arrangement of fascicle attachments reveals the directionality of the tendons. For instance, in pennate muscles, tendinous attachments are linearly arranged, whereas in non-pennate muscle, they are arranged in more diverse patterns. To be more specific, for pennate muscles, the distribution of the attachment points is approximately represented as a long and thin ellipsoid, the principal axis of which roughly matches the tendon axis. The least square regression method can used to find this axis:

$$\min_{\beta_1\beta_2}\sum_i \|S(\mathbf{p}_i) - \boldsymbol{\beta}_1 t_i - \beta_2\|^2 \tag{6}$$

where $S(\mathbf{p})$ denotes the attachment points and $\boldsymbol{\beta}_1 t + \beta_2$ is the linear regression model to fit. The vector $\boldsymbol{\beta}_1$ is the estimated principal axis for the line of action (see Figure 5).

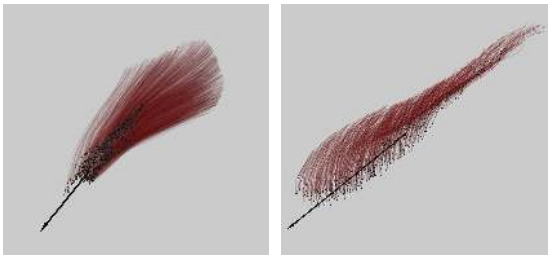

(a) (b)

Figure 5: Estimated line of action (black arrow) and distal attachments (black dots) of fascicles (red) for pennate muscle. (a) Supraspinatus. (b) Vastus medialis.

2.4. Pennate and non-pennate muscles

Depending on pennation, the line of action in (1) is determined by using either (5) or (6). For reliable quantification of PA, the method for determining the line of action must be chosen consistently. To this end, recall that attachments of fascicles are arranged linearly in pennate muscle, but are more complex in non-pennate muscle. To utilize this characteristic in determining the type of muscle, we evaluate the quality of the fit in (6) by considering

$$r^2 = 1 - \frac{\sum_{i=1}^{n}\|S(\mathbf{p}_i) - \boldsymbol{\beta}_1 t_i - \beta_2\|^2}{\sum_{i=1}^{n}\|S(\mathbf{p}_i) - \overline{S(\mathbf{p})}\|^2} \tag{7}$$

where $\overline{S(\mathbf{p})} = \frac{1}{n}\sum_{i=1}^{n} S(\mathbf{p}_i)$ and n is the number of attachment points. Here, $r^2 = 1.0$ indicates a perfect fit of our regression model, while $r^2 = 0.0$ is associated with the poorest fit. Because of the linearity of their attachment arrangement, pennate muscles have high values of r^2, whereas non-pennate muscles have lower values of r^2. Based on this difference, a threshold for the r^2 value can be chosen to classify muscles as either pennate or non-pennate. However, some pennate muscles, which are directly attached to bones without any external tendons, may need to be classified differently. In

such cases, the line of action is approximated as the average orientation of fascicles using (5) instead (see Figure 6). Attachment types (i.e., tendinous or bony attachment) can be determined during the dissection and digitization process.

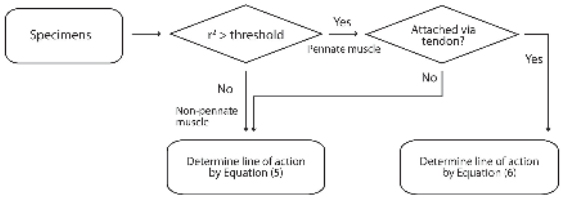

Figure 6: Flow chart for our method to determine the line of action.

2.5. Anatomical reference frame

A reference coordinate frame must be determined to evaluate the correlation between the PA distribution and the fascicles' anatomical positions within the muscle volume. To this end, a three-dimensional Cartesian coordinate system is formed by the three orthogonal axes that originate from the geometric center of the muscle and correspond to the well-known anatomical directions: proximo-distal, superficial-deep and latero-medial (or anterior-posterior) (see Figure 7).

The estimated line of action (described in Section 2.3) is used to represent the proximo-distal axis. Subsequently, the cross-section, π_C, is defined as the plane that is transverse to the proximo-distal axis and located at the origin of the coordinate frame (see Figure 7(b)). The intersection of π_C and the fascicles yields a two-dimensional point-set, $\{S(\mathbf{p}_c)\}$. Many superficial muscles have elliptical cross-sections, the longer and shorter axes of which approximately correspond to the latero-medial and the superficial-deep axes, respectively (See Figure 7(c)). These axes can be effectively estimated by a principal component analysis (PCA): the eigenvector associated with the larger eigenvalue approximates the major axis of the ellipse whereas the eigenvector associated with the smaller eigenvalue represents its minor axis. In the case of muscles that have circular cross-sections (e.g., ECRL), the axes determination may be inconsistent, as those eigenvectors may not coincide with the corresponding anatomical axes. Consequently, manual adjustment may be required. With regard to the proximo-distal axis, all distal attachments of the fascicles are projected onto this axis and their relative positions are used to evaluate correlation. Regarding the latero-medial and superficial-deep axes, the geometric deviations of all fascicles from the center of the muscle are calculated and then assessed in relation to the axes.

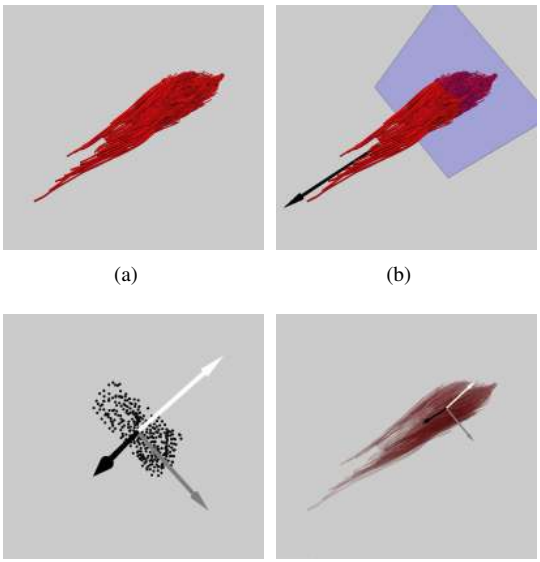

Figure 7: Anatomical reference frame. (a) Fascicles of extensor digitorum muscle. (b) Illustration of the line of action, shown as the black arrow in the distal region, and the corresponding cross-section, π_C, shown as the purple plane. (c) Intersection points of π_C with the fascicles and the estimated anatomical directions, superficial-deep (white arrow) and the medial-lateral (gray arrow). (d) Reference coordinate frame shown with the fascicles.

3. Results

Our statistical results for 18 muscles are given in Table 1. The linearity of the geometric arrangement of the distal attachments is evaluated using (7). All pennate (i.e., unipennate and bipennate) muscles have r^2 values ranging from 0.92 to 0.99, indicating a highly linear arrangement of attachment. Other muscles having lower r^2 values are classified as non-pennate muscles (i.e., fusiform and convergent). A value of 0.9 is selected as the dividing threshold between pennate and non-pennate muscle. However, there exist exceptional cases that may need to be dealt with differently, such as ANC. Although the distal attachment for ANC muscle exhibits a strong linear arrangement ($r^2 = 0.962$), the estimated axis may not represent its tendinous axis, since the ANC muscle is attached directly to the ulna without an external tendon. Consequently, this estimated axis may coincide with the longitudinal axis of the bone. In such cases for which a muscle is attached directly to a bone, the line of action is approximated as an average orientation of fascicles using (5) instead.

Fan-shaped muscles (ANC, PM and PQ) have substan-

Muscle	N	Pattern	r^2	PA (distal attachment)
ABH	396	pennate	0.976	18.85 ± 8.88 (0.67 – 52.05)
ANC	728	non-pennate	0.962	16.79 ± 12.31 (0.48 – 78.81)
APL	620	pennate	0.978	13.10 ± 5.61 (0.57 – 41.99)
BR	182	non-pennate	0.679	2.88 ± 1.96 (0.16 – 10.15)
ECRB	630	pennate	0.936	14.17 ± 4.89 (1.84 – 35.10)
ECRL	629	non-pennate	0.825	11.69 ± 5.05 (0.58 – 31.37)
ECU	449	pennate	0.993	6.41 ± 2.99 (0.39 – 19.04)
ED	460	pennate	0.976	9.06 ± 3.36 (0.63 – 22.21)
EDM	158	pennate	0.998	5.55 ± 2.54 (0.38 – 10.73)
EI	176	pennate	0.989	9.63 ± 4.39 (0.64 – 21.98)
EPB	155	pennate	0.966	22.85 ± 8.85 (9.49 – 49.9)
EPL	201	pennate	0.996	6.36 ± 3.02 (0.78 – 15.75)
FCU	1047	pennate	0.997	15.42 ± 6.93 (0.48 – 37.61)
PM	792	non-pennate	0.787	13.56 ± 10.19 (0.23 – 41.32)
PQ	910	non-pennate	0.699	19.61 ± 10.31 (2.91 – 59.65)
PT	1218	pennate	0.981	15.77 ± 6.89 (0.26 – 41.96)
SS	1750	pennate	0.928	16.51 ± 9.54 (0.38 – 43.91)
VM	703	pennate	0.977	34.51 ± 15.64 (2.63 – 70.03)

Table 1: Estimation of PA. N is the number of digitized fascicles. The value of PA (°) is given as 'the mean ± the standard deviation (min-max)'.

tial variation in their PA, whereas fusiform or parallel muscles (BR, ECRL) have a relatively small range of PA values. In fan-shaped muscles, fascicles are spread over a broad area and converge into a narrow attachment site. The PA is distributed from the fascicles located farthest from the central axis (78.81° in ANC) to ones located closest to this axis (0.48° in ANC). In pennate muscles, fascicles are inserted more obliquely at the distal end of the tendon, whereas they are nearly parallel to the tendon axis at the proximal end.

Our PA estimation results are also presented graphically (see Figures 8, 9, 10 and 11). To effectively visualize the local variation of PA throughout a muscle, its distribution is normalized and mapped onto a color gradient ranging from red (PA_{min}) to blue (PA_{max}). The correlation between region and PA is mathematically quantified by associating the geometric location of the fascicle with the three anatomical axes as described in Section 2.5. With respect to these axes, the distribution of PA is depicted in plots and the observed correlations are expressed using fitted polynomial functions. Our results demonstrate that the correlation patterns may differ from muscle to muscle and furthermore that one axis may have a stronger correlation than another. In relation to the anatomical axes, PA changes either monotonically (e.g., decreasing or increasing) or non-monotonically (e.g., decreasing and then increasing). In most cases, these patterns are well-fitted by either linear or quadratic function.

Among the muscles we studied, the pennate muscles are commonly observed to have increasing PA in the proximo-distal direction. This correlation is stronger for unipennate muscles (e.g., EPB and VM) than for other types of muscles because these unipennate muscles have a relatively simple architectural pattern in that the fascicles are attached to only one side of the tendon (see Figure 8). In contrast, some bipennate muscles (e.g., APL) may have multiple regions corresponding to the architectural pattern or attached tendon, which produce a mixture of correlations, such as a variable rate for an increasing pattern (see Figure 9). The correlation with the proximo-distal direction rarely occurs for non-pennate muscles (e.g., BR and ECRL). Instead, these muscles are observed to have changing pattern of PA in the transverse direction, such as the latero-medial or superficial to deep (see Figure 10). Similarly, in bipennate muscles, PA distribution may be characterized with respect to the latero-medial direction, because, in those muscles, the geometric deviation of fascicles from the line of action (i.e., extramuscular tendon for non-pennate muscles and intramuscular tendon for bipennate muscles) can be quantified in the transverse direction, which is proportional to their PA. Fascicle arrangement may be nearly symmetric (e.g., ECRB) or asymmetric (e.g., APL) in relation to the tendon, which leads to either non-monotonic or monotonic PA distribution (see Figure 11).

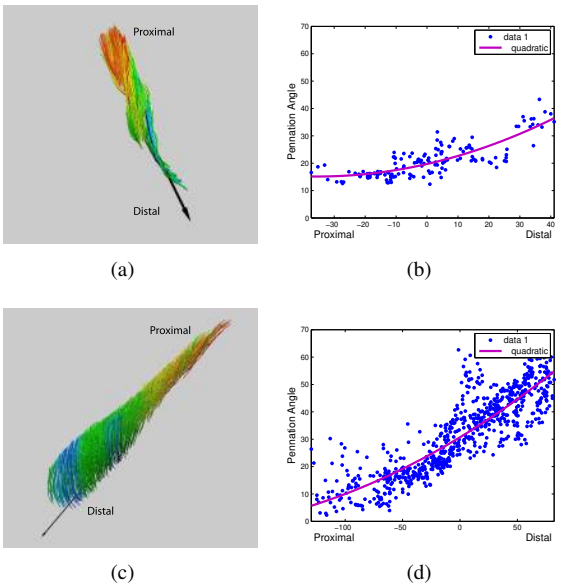

Figure 8: PA variation and its correlation with the proximal-distal direction for unipennate muscles. (a) Entire color field of PA for EPB. (b) PA distribution and its fitted model: $y = 0.0036373\,x^2 + 0.25795\,x + 19.721$. (c) Entire color field of PA for VM. (d) PA distribution and its fitted model: $y = 0.00047506\,x^2 + 0.25476\,x + 30.719$.

4. Discussion

PA is an important architectural parameter used to characterize muscle functions. To determine PA, many biomechanical and clinical studies commonly employ radiological methodologies, which yield an average measurement only for an entire muscle. Thus, the underlying architecture is oversimplified and the associated PA may be underestimated. The purpose of our study is to investigate and quantify the detailed variation of PA reliably over complex architectures. To this end, fascicles were acquired from cadaveric specimens and geometrically reconstructed throughout the muscle volume. Specifically, the geometric arrangement of the fascicle attachments was examined to determine the line of action and fascicle orientation, which were used to estimate PA. As the data used in our study are volumetric, we are able to demonstrate that PA varies regionally throughout a muscle and that this variation may be characterized with respect to the anatomical axes.

Architectural variation has an effect on functional properties of muscle [5, 21]. Thus, uniform architectural models, that many clinical and biomechanical studies are traditionally based on, may impose limits on investigating more complex problems. Our ar-

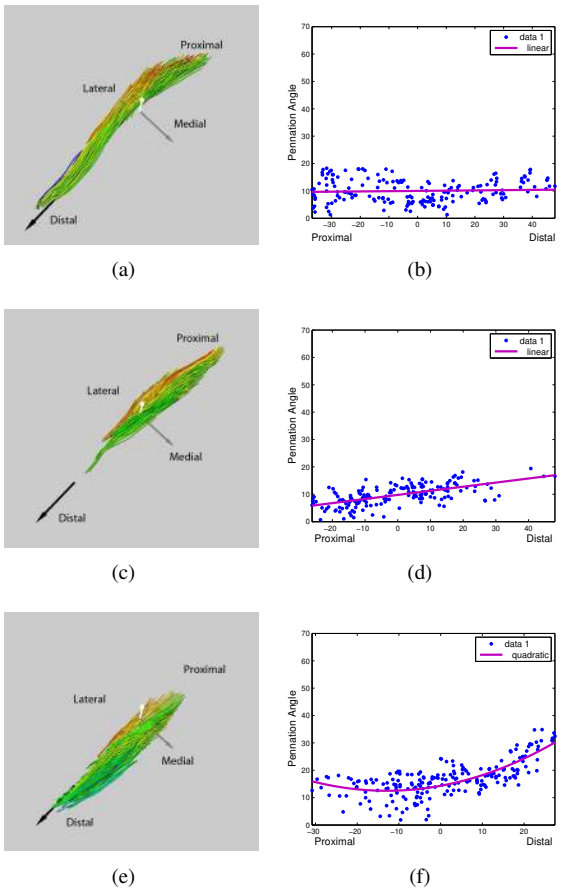

Figure 9: PA variation and its correlation with the proximal-distal direction for bipennate muscles with multiple regions. (a)(c)(e) Color field of PA for APL region 1, 2 and 3, respectively. (b) PA distribution of region 1 (located in the lateral region) and its fitted model: $y = 0.0093577\,x + 10.003$. (d) PA distribution of region 2 (located in the proximal and central region) and its fitted model: $y = 0.14987\,x + 9.774$ (f) PA distribution of region 3 (located in the medial region) and its fitted model: $y = 0.010845\,x^2 + 0.28093\,x + 14.338$. Note that entire color field of PA for APL is shown in Figure 11(c).

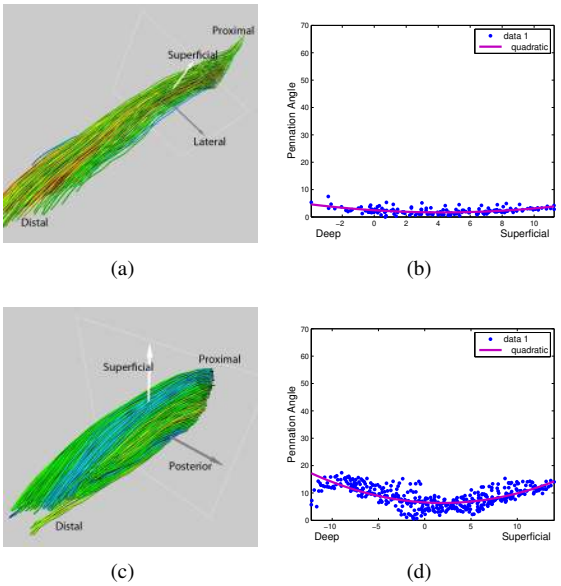

(a) (b)

(c) (d)

Figure 10: PA variation and its correlation with the superficial-deep direction for fusiform muscles. (a) Entire color field of PA for BR. (b) PA distribution and its fitted model: $y = 0.043905\,x^2 - 0.37168\,x + 2.4642$. (c) Entire color field of PA for ECRL. (d) PA distribution and its fitted model: $y = 0.05396\,x^2 - 0.20736\,x + 6.5558$.

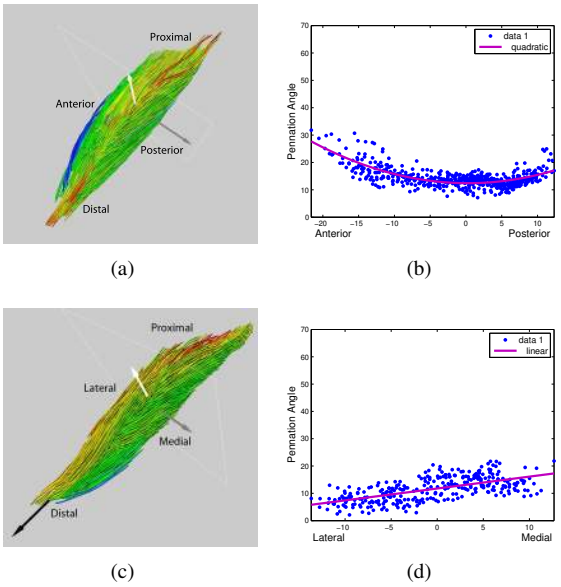

(a) (b)

(c) (d)

Figure 11: PA variation and its correlation with the medial to lateral (or anterior to posterior) direction for bipennate muscles. (a) Entire color field of PA for ECRB. (b) PA distribution and its fitted model: $y = 0.031945\,x^2 - 0.015641\,x + 12.433$. (c) Entire color field of PA for APL. (d) PA distribution and its fitted model: $y = 0.43524\,x + 11.766$.

chitectural model, that accounts for region-specific variation, such as parametric functional PA, could help enhance accuracy for many other studies based on those problems. Moreover, our method may be directly applied to fascicle data that are obtained by diffusion tensor MRI [9, 3]. As this is a non-invasive, *in vivo* methodology, it may be possible to trace a changing PA distribution during muscle contraction, which may provide computational insights for a variety of dynamic problems.

The results obtained from our study and others, such as direct measurement on specimens [11, 12], MRI [18] and ultrasonography [6, 14] are compared in Table 2 and Figure 12. The key differences between our approach and others are:

1. while our analysis is based on the data collected throughout the entire muscle, other studies use only sampled fascicle data,

2. our statistical results are based on the intra-muscular variation whereas those of others are based on the inter-muscular variation.

Consequently, our results yield larger deviation than those of others. The studies that use goniometric measurement of the fascicles on the superficial surface of the muscle, do not take into account the variations that exist within the muscle. Moreover, the limited samples of superficial fascicles may not be sufficient to quantify the complex pattern of PA variation (e.g., ECRB and PT). On the other hand, muscles having little architectural variation (e.g., BR) may compromise this deficiency. For MRI and ultrasonography, the alignment of the scanning plane is a significant factor in the reliable measurement of PA [2, 15]. Furthermore, as the muscle architecture is only assessed longitudinally, it is difficult to account for any variation in the transverse direction.

Although our study provides improved capability for PA estimation, some limitations should be mentioned. First, our analysis does not include the inter-muscular variation of PA. A study of this would require more specimens. Second, only one transverse plane that is positioned at the middle of belly is chosen to evaluate the correlation with the latero-medial or superficial to deep direction. More extensive analysis may need to include other transverse planes at different positions. Last, PA variation is only assessed in relation to an individual axis, which yields a one-dimensional characterization of PA (i.e., $f(x)$). More accurate analysis requires a multi-dimensional characterization of PA (i.e., $f(x, y, z)$).

Muscle	Our method	Other studies
BR	2.88 ± 1.96	2.0 ± 0.6^{a}
ECRB	14.17 ± 4.89	8.9 ± 2.0^{b}
ECRL	11.69 ± 5.05	2.5 ± 0.7^{b}
PQ	19.61 ± 10.31	10.0 ± 0.3^{a}
PT	15.77 ± 6.89	10.0 ± 0.8^{a}
SS	16.51 ± 9.54	12.05 ± 3.07^{c}
VM	34.51 ± 15.64	36 ± 2.15^{d}, $5 - 50^{e}$

Table 2: Comparison of estimated PA for selected muscles. Other studies were based on direct measurement on specimens (a, b) [11, 12], ultrasonography (c, d) [6, 14] and MRI (e) [18]

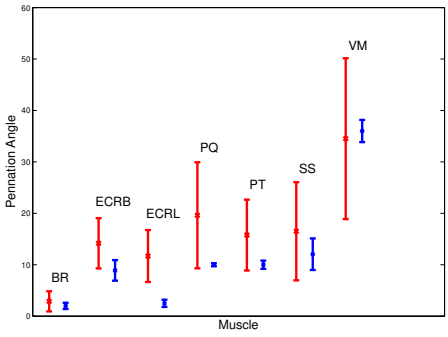

Figure 12: Comparison of estimated PA for selected muscles. Depicted values are given in Table 2. Our results are in red and those of other studies are in blue.

Acknowledgement

This research was supported in part by the Natural Sciences and Engineering Research Council (NSERC) of Canada and the GRAND NCE of Canada.

Conflict of interest statement

We hereby declare that no conflict of interest exists in our study.

Reference

[1] Agur, A., Ng-Thow-Hing, V., Ball, K., Fiume, E., McKee, N., 2003. Documentation and three-dimensional modelling of human soleus muscle architecture. Clinical Anatomy 16, 285–293.

[2] Bénard, M., Becher, J., Harlaar, J., Huijing, P., Jaspers, R., 2009. Anatomical information is needed in ultrasound imaging of muscle to avoid potentially substantial errors in measurement of muscle geometry. Muscle Nerve 39, 652–665.

[3] Froeling, M., Nederveen, A., Heijtel, D., Lataster, A., Bos, C., Nicolay, K., Maas, M., Drost, M., Strijkers, G., 2012. Diffusion-tensor MRI reveals the complex muscle architecture of the human forearm. Journal of Magnetic Resonance Imaging 36, 237–248.

[4] Gans, C., de Vree, F., 1987. Functional bases of fiber length and angulation in muscle. Journal of Morphology 192, 63–85.

[5] Jacobson, M., Raab, R., Fazeli, B., Abrams, R., Botte, M., Lieber, R., 1992. Architectural design of the human intrinsic hand muscles. The Journal of Hand Surgery 17, 804–809.

[6] Kim, S., Boynton, E., Ravichandiran, K., Fung, L., Bleakney, R., Agur, A., 2007. Three-dimensional study of the musculotendinous architecture of supraspinatus and its functional correlations. Clinical Anatomy 20, 648–655.

[7] Koolstra, J., van Eijden, T., Weijs, W., 1989. An iterative procedure to estimate muscle lines of action in vivo. Journal of Biomechenics 22, 911–920.

[8] Lee, D., Ravichandiran, K., Jackson, K., Fiume, E., Agur, A., 2012. Robust estimation of physiological cross-sectional area and geometric reconstruction for human skeletal muscle. Journal of Biomechanics 45, 1507–13.

[9] Levin, D.I., Gilles, B., Madler, B., Pai, D.K., 2011. Extracting skeletal muscle fiber fields from noisy diffusion tensor data. Medical Image Analysis 15, 340–353.

[10] Lieber, R., Friden, J., 2000. Functional and clinical significance of skeletal muscle architecture. Muscle Nerve 23, 1647–1666.

[11] Lieber, R.L., Fazeli, B.M., Botte, M.J., 1990. Architecture of selected wrist flexor and extensor muscles. The Journal of Hand Surgery 15, 244–250.

[12] Lieber, R.L., Jacobson, M.D., Fazeli, B.M., Abrams, R.A., Botte, M.J., 1992. Architecture of selected muscles of the arm and forearm: Anatomy and implications for tendon transfer. The Journal of Hand Surgery 17, 787–798.

[13] Murray, W.M., Buchanan, T.S., Delp, S.L., 2000. The isometric functional capacity of muscles that cross the elbow. Journal of Biomechanics 33, 943–952.

[14] O'Brien, T., Reeves, N., Baltzopoulos, V., Jones, D., Maganaris, C., 2010. Muscle-tendon structure and dimensions in adults and children. Journal of Anatomy 216, 631–642.

[15] Rana, M., Wakeling, J., 2011. In-vivo determination of 3D muscle architecture of human muscle using free hand ultrasound. Journal of Biomechanics 44, 2129–2135.

[16] Ravichandiran, K., Ravichandiran, M., Oliver, M., Singh, K., McKee, N., Agur, A., 2009. Determining physiological cross-sectional area of extensor carpi radialis longus and brevis as a whole and by regions using 3D computer muscle models created from digitized fiber bundle data. Comput. Methods Prog. Biomed. 95, 203–212.

[17] Rosatelli, A., Ravichandiran, K., Agur, A., 2008. Three-dimensional study of the musculotendinous architecture of lumbar multifidus and its functional implications. Clinical Anatomy 21, 539–546.

[18] Scott, S., Engstrom, C., Loeb, G., 1993. Morphometry of human thigh muscles. Determination of fascicle architecture by magnetic resonance imaging. Journal of Anatomy 182, 249–257.

[19] van Spronsen, P.H., Valk, J., Weijs, W.A., Prahl-Andersen, B., 1987. Analysis of masticatory muscle orientation in adults by means of MRI. Acta Anatomica 130, 96–97.

[20] Van Donkelaar, C., Kretzers, L., Bovendeerd, P., Lataster, L., Nicolay, K., Janssen, J., Drost, M., 1999. Diffusion tensor imaging in biomechanical studies of skeletal muscle function. Journal of Anatomy 194, 79–88.

[21] Van Eijden, T., Korfage, J., Brugman, P., 1997. Architecture of the human jaw-closing and jaw-opening muscles. The Anatomical Record 248, 464–474.

[22] Ward, S., Kim, C., Eng, C., Gottschalk, L., Tomiya, A., Garfin, S., Lieber, R., 2009. Architectural analysis and intraoperative measurements demonstrate the unique design of the multifidus muscle for lumbar spine stability. J Bone Joint Surg Am 91, 176–185.

[23] Zajac, F., 1989. Muscle and tendon: properties, models, scaling, and application to biomechanics and motor control. Critical Reviews in Biomedical Engineering 17, 359–411.